Establishing the Principles of Recognition in the Adenine-Binding Region of an Aminoglycoside Antibiotic Kinase [APH(3′)-IIIa]†

David D. Boehr,‡,§ Adam R. Farley,||,⊥ Frank J. LaRonde,‡ Tera Rica Murdock,|| Gerard D. Wright,‡ and James R. Cox*,||

Antimicrobial Research Centre, Department of Biochemistry and Biomedical Sciences, McMaster University, Hamilton, Ontario, Canada L8N 3Z5, and Department of Chemistry, Murray State University, Murray, Kentucky 42071

Received June 7, 2005; Revised Manuscript Received July 18, 2005

ABSTRACT: The protein-based molecular recognition of the adenine ring has implications throughout biological systems. In this paper, we discuss the adenine-binding region of an aminoglycoside antibiotic kinase [APH(3′)-IIIa], which serves as an excellent model system for proteins that bind the adenine ring. This enzyme employs a hydrogen-bonding network involving water molecules along with enzyme backbone/side-chain atoms and a $\pi-\pi$ stacking interaction to recognize the adenine ring. Our approach utilized site-directed mutagenesis, adenosine analogues and a variety of biophysical methods to probe the contacts in the adenine-binding region of APH(3′)-IIIa. The results point to the polar nature of an adenine-Met90 contact in this binding pocket and the important role that Met90, the "gatekeeper" residue in structurally similar Ser/Thr protein kinases, plays in adenine binding. The results also suggest that small changes in the structure of the adenine ring can lead to significant changes in the ability of these analogues to occupy the adenine-binding region of the enzyme. Additional computational experiments indicate that both size and electronic factors are important in the binding of aromatic systems in this interaction-rich pocket. The principles governing adenine recognition established in this study may be applied to other protein−ligand complexes and used to navigate future studies directed at discovering potent and selective inhibitors of APH-type enzymes.

Adenosine 5′-triphosphate (ATP)[1] plays critical roles across all forms of life, and delineating the molecular forces that contribute to the protein-mediated recognition of the adenine ring is essential to understanding protein function and for drug design. A recent data mining study of the Protein Data Bank (PDB) demonstrated that the most common noncovalent interactions involved in binding between proteins and the adenine ring are hydrogen-bonding, $\pi-\pi$ stacking, and cation$-\pi$ interactions (*1*). One enzyme that typifies the majority of these structural motifs is aminoglycoside 3′-phosphotransferase [APH(3′)-IIIa], a well-studied aminoglycoside phosphotransferase that is important for antibiotic drug resistance (*2*).

The $\pi-\pi$ stacking interaction between Tyr42 of APH(3′)-IIIa and its nucleotide ligands also means that the protein can serve as a model system to understand $\pi-\pi$ stacking interactions between proteins and ligands in general. There is a very high prevalence of aromatic ring systems among pharmaceutical compounds that are involved in a variety of π interactions with their target proteins (e.g., acetylcholinesterase and the drug "Aricept") (*3*, *4*). Although much is known about $\pi-\pi$ interactions in model systems of small molecules, little thermodynamic information is available for biologically relevant systems, and it is not known how other interactions available in proteins (e.g., hydrogen bonds) may modulate these ligand interactions (*4*).

Previous thermodynamics analyses have demonstrated that the $\pi-\pi$ stacking interaction between APH(3′)-IIIa and the adenine ring of adenosine 5′-diphosphate (ADP)/adenosine 5′-(β,γ-imino)triphosphate (AMPPNP) can supply up to one-third of the total nucleotide-binding energy (*5*, *6*). This is especially important because the APHs are structurally similar to eukaryotic protein kinases (ePKs) (*7*), which lack a similar $\pi-\pi$ stacking interaction (*5*). A thermodynamic comparison of nucleotide binding to wild-type APH(3′)-IIIa and Tyr42 mutants demonstrated that nucleotide binding to APH(3′)-IIIa is an enthalpy-driven event with important electrostatic considerations (*6*).

Many ePKs are important pharmacological targets (*8*−*10*), and the large number of compound libraries de-

† This research was supported by a grant from the Canadian Institutes of Health Research to G.D.W. (MT-13536) and a grant from the American Chemical Society−Petroleum Research Fund to J.R.C. (39738-B). G.D.W. holds a Canada Research Chair in Antibiotic Biochemistry.

* To whom correspondence should be addressed: Department of Chemistry, Murray State University, 456 Blackburn Science, Murray, KY 42071-3346. Telephone: 270-762-6543. Fax: 270-762-6474. E-mail: ricky.cox@murraystate.edu.

‡ McMaster University.

§ Present address: Department of Molecular Biology, The Scripps Research Institute.

|| Murray State University.

⊥ Present address: Department of Biochemistry, Vanderbilt University.

[1] Abbreviations: APH(3′)-IIIa, aminoglycoside 3′-phosphotransferase; ATP, adenosine 5′-triphosphate; ADP, adenosine 5′-diphosphate; AMPPNP, adenosine 5′-(β,γ-imino)triphosphate; PDB, Protein Data Bank; NADH, nicotinamide adenine dinucleotide reduced; ES-MS, electrospray mass spectrometry; ITC, isothermal titration calorimetry; ePK, eukaryotic protein kinase; TAR, 1,2,3,5-tetra-*O*-acetyl-β-D-ribofuranose.

10.1021/bi051085p CCC: $30.25
Published on Web 08/25/2005

signed against these targets may contain potent APH inhibitors. However, the structural similarity between protein classes means that it will be important to ensure that the APH inhibitors are not cross-reactive to human kinases. The best inhibitors of ePK function target primarily the adenine-binding region (*11*, *12*), including ePK inhibitors in clinical development (*9*, *10*), and it is likely that potent inhibitors of APHs will need to take advantage of the binding opportunities available in this deep, interaction-rich pocket. Thus, a clear and complete understanding of the requirements for tight binding in the adenine-binding pocket of APHs and an appreciation of the differences in the adenine-binding pockets between APHs and ePKs, including the $\pi-\pi$ stacking interaction in APH(3′)-IIIa, are important steps forward in the design of potent inhibitors of APHs capable of reversing antibiotic resistance *in vivo*.

In this paper, we provide a further assessment of the nature and energetics of the contacts in the adenine-binding region of APH(3′)-IIIa and discuss the role of electrostatic interactions in the enzyme-mediated recognition of the adenine ring. A part of our efforts focuses on the interaction between Met90 and the adenine ring. This interaction is important not only for understanding ligand interactions with APH(3′)-IIIa, but the equivalent residue in protein kinases, the "gatekeeper residue", determines in large part the inhibitor sensitivity of the various kinases. Using APH(3′)-IIIa as a model for ePKs has been recently exemplified by Shokat's group in a study paralleling our own in demonstrating the importance of Met90 to APH(3′)-IIIa function (*13*). This study will add considerably to the existing bioinformatics-based information on the packing of the adenine ring in protein structures and the nature of $\pi-\pi$ stacking interactions, in particular, between proteins and their ligands (*1*, *4*, *6*, *14*).

MATERIALS AND METHODS

Reagents. Kanamycin A was from Bioshop (Burlington, Ontario, Canada). All other chemicals and adenosine analogues were purchased from Sigma (St. Louis, MO) unless otherwise noted. All oligonucleotide primers were synthesized at the Central Facility of the Institute for Molecular Biology and Biotechnology, McMaster University. The purification of APH(3′)-IIIa has been described previously (*15*), and the mutant enzymes were purified in an analogous manner.

Electrostatic Potential Surface Calculations on the APH(3′)-IIIa Adenine-Binding Pocket and Adenosine Analogues. The coordinates of Tyr42, Met90, Ser91, Glu92, Ala93, Phe197, and Ile207 of APH(3′)-IIIa were extracted from the PDB file of the APH(3′)-IIIa−ADP complex (PDB code 1J7L). The 90−93 peptide fragment was left intact, and the resulting termini were capped with methyl groups. Only the side chains of Tyr42, Phe197, and Ile207 were used in the calculations below, which were terminated with the addition of hydrogen atoms to fill open valences. This model of the adenine-binding pocket was investigated using Density Functional Theory (B3LYP/6-31G**) with all atoms remaining fixed in their crystallographically determined positions. Two calculations were performed with this system, where the adenine ring (N9-methyl adenine) was either bound or absent in the binding pocket. Electrostatic potential surfaces were generated by mapping the 6-31G** potentials onto surfaces of molecular electron density. The areas in red represent negative electrostatic potentials, and the areas in blue represent positive electrostatic potentials.

Model systems of the adenosine analogues were generated by taking the coordinates of ADP from the same crystal structure and deleting all of the atoms except for the atoms in the adenine ring, the anomeric carbon, and the oxygen atom in the ribose ring. All valences were filled with hydrogen atoms. In silico, modification of the adenine ring resulted in the different heteroaromatic systems found in the adenosine analogues. Calculations utilizing Density Functional Theory (B3LYP/6-31G**) and *ab initio* calculations at the HF/6-31G** level of theory were performed on the heteroaromatic adenosine analogues, and the 6-31G** potentials were mapped onto surfaces of molecular electron density. For each analogue, the two types of calculations yielded similar potential maps. All calculations were performed in Spartan '04 (Wavefunction, Inc., Irvine, CA). The potential energy extremes in the electrostatic maps are from −25 to +25 kcal/mol. The color red indicates areas of greater electron density, while the color blue indicates areas of less electron density. From negative to positive potentials, the colors progress red−orange−yellow−green−cyan−blue.

Site-Directed Mutagenesis. Site-directed mutagenesis was performed using the QuikChange method (Stratagene, La Jolla, CA). The appropriate mutagenic primers (Met90Ala, 5′-GGAGCAATCTGCTCGCGAGTGAGGCC; Met90Leu, 5′-GGAGCAATCTGCTCT-TGAGTGAGGCC) and their reverse complements were used in combination with 20 ng of template DNA (pETSACG1) in Pfu DNA polymerase (Stratagene, La Jolla, CA) catalyzed PCR reactions. After parental DNA was digested with *Dpn*I, mutant plasmid DNA was transformed into $CaCl_2$-competent *Escherichia coli* XL-1 Blue. Plasmids from positive clones were sequenced in their entirety and then used to transform *E. coli* BL21(DE3) for subsequent protein purification.

Enzyme Kinetic Assays. The phosphotransferase assay employed has previously been described (*15*). The assay measures the production of ADP, generated upon aminoglycoside phosphorylation, and couples that production to the oxidation of β-nicotinamide adenine dinucleotide reduced (NADH) using the enzymes pyruvate kinase and lactate dehydrogenase. The rate of ADP production was determined by monitoring the decrease in absorbance at 340 nm. Initial rates were fit to the Michaelis−Menten eq 1 using Grafit 4.0 (Erithacus Software, Staines, U.K.).

$$v = (k_{cat}/E_t)[S]/(K_M + [S]) \quad (1)$$

Isothermal Titration Calorimetry (ITC). All of the ITC experiments were performed as previously described on a VP-ITC instrument from Microcal, Inc. (Northampton, MA) (*6*). The titrations were conducted at 30 °C in 50 mM HEPES-NaOH at pH 7.5, 40 mM KCl, and 10 mM $MgCl_2$. The proteins were dialyzed completely against buffer, and the buffer was used to dissolve the ligands. The protein concentration in the sample cell of the calorimeter was 15−60 μM, and the ligand concentration in the syringe was 0.2−6.0 mM, depending on the affinity between the protein and ligand. The experimental titrations were corrected for by subtracting the heat of dilution for the ligand into buffer.

Scheme 1

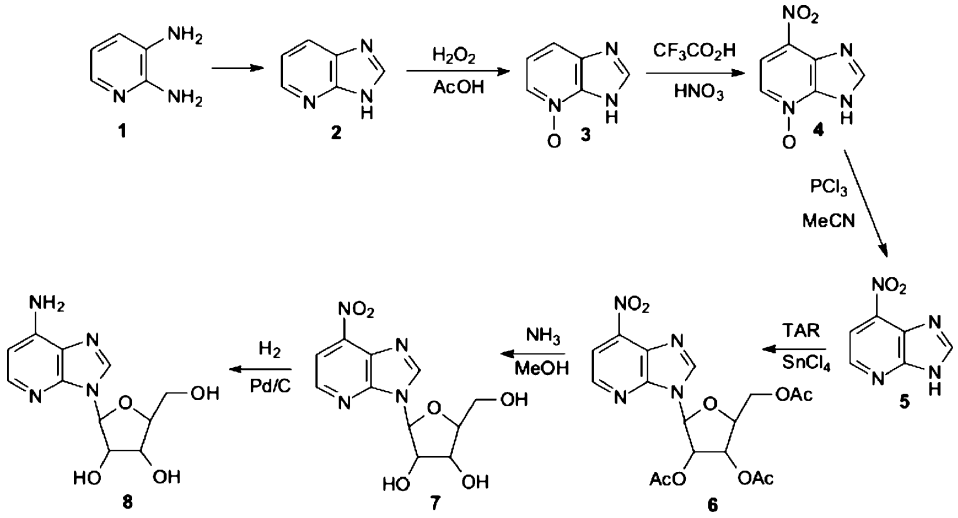

The heat of dilution for the protein was found to be negligible. The binding data was then analyzed using Origin software (*16*). The dissociation constant K_d and the enthalpy change ΔH were used to calculate the free-energy change ΔG and the entropy change ΔS according to the relations in eq 3.

$$-RT \ln(1/K_d) = \Delta G = \Delta H - T\Delta S \qquad (3)$$

*Synthesis of 1-Deazaadenosine (**8**).* Scheme 1 shows the synthesis of 1-deazaadenosine (**8**), which was carried out following previously established methods (*17*, *18*). Mass spectrometry of the products was performed on an Applied Biosystems Q Trap LC−MS system, and ^{1}H NMR experiments were carried out on a Bruker 500 MHz instrument.

*3H-Imidazo[4,5-b]pyridine (**2**).* A mixture of 2,3-diaminopyridine (**1**) (5 g, 45.82 mmol) and triethylorthoformate (100 mL, 601.21 mmol) was refluxed for 3 h. The solution was evaporated to dryness *in vacuo*, and then the residue was heated at reflux with 200 mL of concentrated hydrochloric acid for 1 h. The mixture was allowed to cool, neutralized with solid Na_2CO_3, and extracted with ethyl acetate (3 × 10 mL). The combined organic extracts were dried with Na_2SO_4 and filtered, and the solvent was removed at reduced pressure. The residue was dissolved in absolute ethanol, treated with charcoal, and filtered, and then the solvent was evaporated to give 4.3 g (80%) of desired product, mp 152−154 °C. ^{1}H NMR (DMSO-d_6) δ: 8.54 (s, 1H, H-2), 8.45 (d, 1H, J = 5 Hz, H-5), 8.11 (d, 1H, J = 8 Hz, H-7), 7.3 (m, 1H, H-6). Electrospray mass spectrometry (ES-MS) calculated for $C_6H_5N_3$, 119.1; found, 120.0 $(M + H)^+$.

*Imidazo[4,5-b]pyridine-N-oxide (**3**).* To a solution of 3H-imidazo[4,5-b]pyridine (**2**) (4 g, 33.58 mmol) in glacial acetic acid (30 mL) was added aqueous hydrogen peroxide (30%, 30 mL). The mixture was heated in a water bath at 70−80 °C. After 3 h, an additional 2.5 mL of hydrogen peroxide solution was added, and the mixture was maintained an additional 9 h at the same temperature. The mixture was concentrated to about 10 mL *in vacuo*, whereupon a product precipitated from the solution. The product was filtered-off and washed with water (5 mL). This produced 3.86 g (86%) of the desired product. ES-MS calculated for $C_6H_5N_3O$, 135.1; found, 135.9 $(M + H)^+$.

*4(7)-Nitropyrimidineimidazole-4-oxide (**4**).* To a solution of imidazo[4,5-b]pyridine-*N*-oxide (**3**) (3.5 g, 25.91 mmol) in trifluoroacetic acid (25 mL) at 0 °C was added, in a dropwise manner, 70% fuming nitric acid (22 mL). The mixture was heated at 90 °C for 3 h, cooled, and then poured onto crushed ice. The mixture was neutralized with concentrated ammonium hydroxide while maintaining the temperature below 30 °C. The resulting solid was filtered, washed with ice water, and dried to give 1.2 g (26%) of product as light yellow needles. ^{1}H NMR (DMSO-d_6) δ: 7.34 (s, 1H, NH), 7.24 (s, 1H, H-2), 7.10 (d, 1H, J = 7.0 Hz, H-5), 6.92 (d, 1H, J = 7.2 Hz, H-7). ES-MS calculated for $C_6H_4N_4O_3$, 180.1; found, 180.9 $(M + H)^+$.

*4(7)-Nitropyridineimidazole (**5**).* To a solution of 4(7)-nitropyridineimidazole 4-oxide (**4**) (0.50 g, 2.78 mmol) in dry acetonitrile (10 mL) was added dropwise phosphorus trichloride (2.2 mL), and the mixture was heated at 80 °C for 2 h. After cooling, a yellow solid precipitated, which was collected by filtration and washed with ether and then with saturated sodium-carbonated solution. Recrystallization from water provided 0.07 g (15%) of product as a yellow solid. ^{1}H NMR (DMSO-d_6) δ: 7.43 (s, 1H, H-2), 7.32 (s, 1H, NH), 7.31 (d, 1H, J = 7.2 Hz, H-5), 6.63 (d, 1H, J = 7.2 Hz, H-7). ES-MS calculated for $C_6H_4N_4O_2$, 164.1; found, 164.9 $(M + H)^+$ and 162.8 $(M - H)^-$.

*1-(2′,3′,5′-Tri-O-acetyl-β-D-ribofuranosyl)4-nitropyridineimidazole (**6**).* To a solution of 4(7)-nitropyridineimidazole (**5**) (0.3 g, 1.83 mmol) in dry acetonitrile (10 mL) and 1,2,3,5-tetra-*O*-acetyl-β-D-ribofuranose (TAR, 0.58 g, 1.83 mmol) was added dropwise freshly distilled stannic chloride (0.43 mL, 3.66 mmol), and the solution was stirred at room temperature for 7 h. The reaction mixture was cooled in an ice bath, and the resulting solid was neutralized with $NaHCO_3$ in water and then extracted several times with chloroform. The combined organic layers were dried, filtered, and evaporated to dryness. The residue was chromatographed on silica gel eluting with chloroform/methanol (9:1) to give 0.63 g (82%) of product as light yellow needles (R_f = 0.88). ^{1}H NMR (MeOH) δ: 8.98 (s, 1H, H-2), 8.63 (d, 1H, J = 5.4 Hz, H-6), 8.03 (d, 1H, J = 5.4 Hz, H-5), 6.53 (d, 1H, J

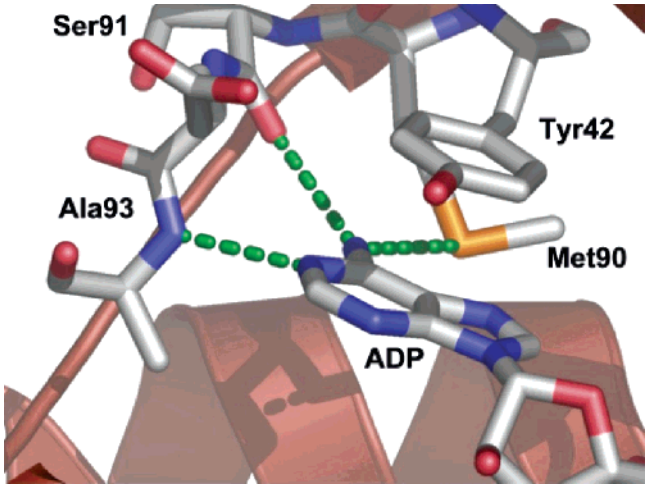

FIGURE 1: Major contacts in the adenine-binding region of APH(3′)-IIIa. Hydrogen bonds are represented by the dashed green lines and are drawn between the amide group of Ala93 and N1 of the adenine ring as well as the amino group of the adenine ring and the carbonyl group of Ser91 and the side chain of Met90. The $\pi-\pi$ stacking interaction between Tyr42 of the enzyme and the adenine ring of the bound nucleotide is also shown.

= 4.6 Hz, H-1′), 5.70 (m, 1H, H-3′), 4.40 (m, 3H, H-4′ and CH_2-5′), 2.03, 2.06, 2.15 (3s, 9H, $COCH_3$). ES-MS calculated for $C_{17}H_{18}N_4O_9$, 422.4; found, 423.1 $(M + H)^+$.

*7-Nitro-3-β-D-ribofuranosyl-3H-imidazo[4,5-b]pyridine (**7**).* A solution of **6** (0.47 g, 1.11 mmol) in methanol (15 mL), saturated at 0 °C with ammonia, was set aside at room temperature for 24 h. The solvent was removed *in vacuo* and the residue was chromatographed on a silica gel column and eluted with EtOAc/MeOH (85:15) to give 0.28 g (86%) of desired product ($R_f = 0.28$) as a yellow powder. ^{1}H NMR (MeOD) δ: 9.00 (s, 1H, H-2), 8.65 (d, 1H, J = 5.4 Hz, H-5), 8.04 (d, 1H, H-6), 6.70 (d, 1H, J = 4.6 Hz, H-1′), 4.71 (m, 1H, H-2′), 4.35 (m, 1H, H-3′), 4.05 (m, 1H, H-4′), 3.71 (m, 2H, CH_2-5′). ES-MS calculated for $C_{11}H_{12}N_4O_6$, 296.2; found, 296.9 $(M + H)^+$.

*7-Amino-3-β-D-ribofuranosyl-3H-imidazo[4,5-b]pyridine (1-Deazaadenosine) (**8**).* To a solution of **7** (60 mg, 0.20 mmol), MeOH (10 mL) was added 10% Pd/C (30 mg), and the mixture was shaken with hydrogen at 30 psi for 1.0 h. The catalyst was removed by filtration, and the filtrate was evaporated to give 50.3 mg (95%) of **8** as colorless crystals, mp 262.3−263.5 °C. ^{1}H NMR (MeOD) δ: 8.99 (s, 1H, H-2), 8.63 (d, 1H, J = 5.4 Hz, H-5), 8.03 (d, 1H, H-6), 6.23 (d, 1H, J = 4.6 Hz, H-1′), 4.71 (m, 1H, H-2′), 4.35 (m, 1H, H-3′), 4.05 (m, 1H, H-4′), 3.83 (m, 2H, CH_2-5′). ES-MS calculated for $C_{11}H_{14}N_4O_4$, 266.3; found, 267.0 $(M + H)^+$.

RESULTS

Electrostatic Description of the Adenine-Binding Pocket in APH(3′)-IIIa. A summary of the major contacts in the adenine-binding region of APH(3′)-IIIa is shown in Figure 1. These include the $\pi-\pi$ stacking interaction involving Tyr42 and hydrogen-bonding interactions with backbone atoms of Ser91 and Ala93 and the side chain of Met90. This hydrogen-bonding scheme involving N1 and N6 of adenine and the backbone atoms of the protein is a common motif in adenine-binding proteins (*1*). Not shown are other potentially important hydrogen bonds between N3 of the adenine ring and water molecules at the mouth of the adenine-binding pocket and N7 of the adenine ring with water molecules that remain in the active site after the nucleotide binds (*6*).

To better understand the interaction of the adenine ring with APH(3′)-IIIa, an electrostatic potential surface of the adenine-binding pocket was generated. This potential map is shown in Figure 2A, with the locations of the atoms involved in hydrogen bonds with the adenine ring highlighted. The positions of all of the atoms in this figure were derived from the X-ray structure of the APH(3′)-IIIa−ADP complex (*5*). The potential map of the adenine-binding pocket provides a qualitative description of the environment encountered by the adenine ring when entering the pocket. To block the entry of ATP into this region of the active site, it is necessary to understand the forces of attraction that can dictate the potency of potential inhibitors. With this in mind, the arrangement of atoms in Figure 2A suggests that electrostatic complementarity between the adenine ring (or an inhibitor) and residues 90−93 of the enzyme may be a key feature for recognition in this binding pocket. A similar calculation was performed with adenine inside the binding pocket, and the results support the idea that the matching of electrostatic extrema plays an important role in placing the adenine ring inside its binding pocket (Figure 2B). In this case, the electronegative N1 atom of the adenine ring (−0.480) is projected toward the electropositive amide hydrogen atom of Ala93 (+0.417), and the electropositive amino hydrogen atoms of the adenine ring (+0.389 and +0.298) are projected toward areas of negative charge near the oxygen atom of Ser91 (−0.552) and sulfur atom of Met90 (−0.201). These results are consistent with the polar nature of hydrogen-bonding interactions in biological molecules (*19*, *20*) and suggest that the contact between adenine and the gatekeeper residue Met90 is more than a hydrophobic interaction.

Contributions of Met90 to Adenosine Binding. The conservation of the ATP-binding pocket in ePKs has made it difficult to design specific inhibitors. In general, any inhibitor selectivity is the result of the lack of conservation of the gatekeeper residue. In the APH(3′) family, this residue is only partially conserved (Figure 3), where this position can also be Thr. The mutation of Met90 to Ala had only minor effects on the steady-state kinetic parameters for ATP and the aminoglycoside kanamycin A, where the largest effect was a 2-fold decrease in k_{cat} (Table 1). There were slightly more significant effects when Met90 was mutated to Leu. The K_M for ATP in APH(3′)-IIIa closely matches the K_d for ATP (*21*, *22*), and thus, the 3.6-fold increase in K_M for ATP with APH(3′)-IIIa Met90Leu suggests a loss of affinity for the nucleotide with this mutant. The K_M for the aminoglycoside is comprised of a number of rate constants, making the minor changes in the steady-state kinetic parameters for kanamycin difficult to decipher.

Our structural analysis of the adenine-binding pocket of APH(3′)-IIIa suggested that Met90 plays an important role in nucleotide association. Thus, to look more closely at this interaction, we compared adenosine binding to wild-type (WT) and Met90 mutant proteins using ITC. ITC is a powerful method that directly measures the enthalpy of binding and can give a full thermodynamic profile of the interaction (*23*, *24*).

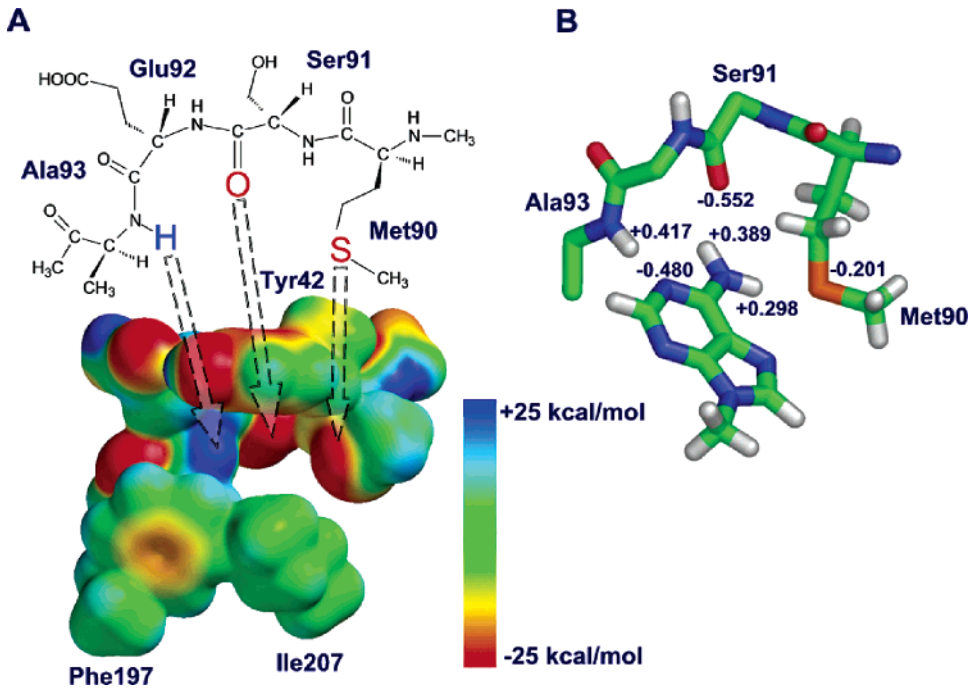

FIGURE 2: (A) Electrostatic potential surface of the adenine-binding pocket of APH(3′)-IIIa. All of the heteroatoms in this figure were derived from the crystal structure of the APH(3′)-IIIa−ADP complex (5). The potential energy extremes in the electrostatic map are from −25 to +25 kcal/mol. The color red indicates areas of greater electron density, while blue indicates areas of less electron density. From negative to positive potentials, the colors progress red−orange−yellow−green−cyan−blue. (B) Selected atoms of the adenine-binding pocket with partial charges derived from the DFT calculation with bound adenine. Only the atoms involved in hydrogen-bonding interactions (see Figure 1) are labeled with a partial charge.

Protein Kinases								
PKA	**117-**	**Y**	**M**	**V**	**M**	**E**	**Y**	**V**
CsK	**82-**	**V**	**L**	**V**	**I**	**D**	**L**	**L**
MAPK	**100-**	**Y**	**I**	**V**	**Q**	**D**	**L**	**M**
PhK	**100-**	**F**	**L**	**V**	**F**	**D**	**L**	**M**
Aminoglycoside Kinases								
APH(3')-IIIa	**87-**	**N**	**L**	**L**	**M**	**S**	**E**	**A**
APH(3')-Ia	**95-**	**W**	**L**	**L**	**T**	**T**	**A**	**I**
APH(3')-Ib	**95-**	**W**	**L**	**L**	**T**	**T**	**A**	**I**
APH(3')-IIa	**91-**	**W**	**L**	**L**	**L**	**G**	**E**	**Y**
APH(3')-IVa	**87-**	**Y**	**L**	**L**	**M**	**E**	**A**	**L**
APH(3')-Va	**87-**	**W**	**L**	**V**	**T**	**E**	**A**	**V**
APH(3')-VIa	**84-**	**F**	**M**	**I**	**T**	**K**	**A**	**I**
APH(3')-VIIa	**78-**	**Y**	**L**	**I**	**M**	**S**	**E**	**I**
					*			

FIGURE 3: Sequence alignment of the gatekeeper residue (boxed) in aminoglycoside and protein kinases.

Although the K_d for adenosine with the Met90Ala (20.3 ± 0.05 μM) was similar to the value with WT APH(3′)-IIIa (11.0 ± 0.1 μM), the enthalpy and entropy contributions were significantly different (Table 2). Adenosine binding to APH(3′)-IIIa WT is an enthalpy-driven event with unfavorable entropy. In contrast, the reverse is true with both the Met90Ala and Met90Leu mutants because entropy is more favorable and enthalpy makes a lower contribution to binding (Table 2). This is especially apparent with APH(3′)-IIIa Met90Leu, where even though the Gibbs free energy of binding is only 1 kcal/mol less (4.7-fold reduction in K_d) than the WT value, the enthalpy contribution is diminished by almost 14 kcal/mol (Table 2). These results suggest that mutation of Met90 significantly changes the energetic contributions to adenosine binding.

Binding of Adenosine Analogues to APH(3′)-IIIa. Another way to investigate the relative importance of the contacts illustrated in Figure 1 is to use adenosine analogues, where the adenine ring has been modified by the addition or deletion of groups or atoms. ITC was used to monitor the binding of the adenosine analogues to WT APH(3′)-IIIa (Table 3, see Figure 4 for an example titration), and the results are in good agreement with the kinetic analysis using the same compounds as enzyme inhibitors (data not shown). The only difference among these nucleosides is the nature of the heteroaromatic system, and changes in the binding constant and thermodynamic parameters can be attributed to the ability of the enzyme to interact with the modified nucleobases. Figure 5 shows the aromatic moieties of the modified analogues and their electrostatic potential surfaces.

Removal of specific sp^2-hybridized N atoms from the adenine ring led to adenosine analogues that bind less tightly to the enzyme (Table 3). The effect was more modest upon removal of N7 and N3, while the replacement of N1 with a C−H group had a devastating effect on complex formation. Thermodynamic analysis with this series of compounds (adenosine, 3-deazaadenosine, and 7-deazaadenosine) demonstrates that, as electron density shifts from polar sites along the edge toward the center of the adenine ring (Figure 5), the affinity and, more specifically, the enthalpy contribution decreases substantially (Table 3).

The ITC experiments with 1-deazaadenosine revealed no binding of this analogue to the enzyme. The lack of complex formation between APH(3′)-IIIa and 1-deazaadenosine can be attributed to the increased size of the ring system and a steric clash between the amide N−H bond of Ala93 and the H−C bond at position 1 in the deaza analogue, which would

Table 1: Steady-State Kinetic Parameters for APH(3′)-IIIa WT and Met90 Mutants

	K_M (μM)	k_{cat} (s^{-1})	k_{cat}/K_M (M^{-1} s^{-1})	K_M^{mut}/K_M^{WT}	$k_{cat}^{WT}/k_{cat}^{mut}$	$(k_{cat}/K_M)^{WT}/(k_{cat}/K_M)^{mut}$
WT[a]						
ATP	27.7 ± 3.7	1.76 ± 0.08	6.35×10^4			
kanamycin A	12.6 ± 2.6	1.79 ± 0.08	1.42×10^5			
Met90Leu						
ATP	98.9 ± 13.4	1.37 ± 0.06	1.39×10^4	3.6	1.3	4.6
kanamycin A	25.9 ± 4.7	2.12 ± 0.11	8.17×10^4	2.1	0.84	1.7
Met90Ala						
ATP	26.1 ± 3.3	0.867 ± 0.025	3.32×10^4	0.94	2.0	1.9
kanamycin A	20.9 ± 3.1	1.22 ± 0.05	5.84×10^4	1.7	1.5	2.4

[a] Values taken from ref *7* for ATP and ref *15* for kanamycin A.

Table 2: Thermodynamics Parameters for Interactions between Adenosine and APH(3′)-IIIa Met90 Mutants[a]

protein	K_d (μM)	ΔG (kcal/mol)	ΔH (kcal/mol)	$-T\Delta S$ (kcal/mol)
wild type	11.0 ± 0.1	−6.88 ± 0.01	−17.5 ± 0.07	+10.6 ± 0.08
Met90Leu	51.9 ± 3.4	−5.94 ± 0.04	−3.73 ± 0.51	−2.21 ± 0.47
Met90Ala	20.3 ± 0.05	−6.51 ± 0.01	−6.37 ± 0.06	−0.14 ± 0.06

[a] The values determined in 50 mM HEPES-NaOH at pH 7.5, 40 mM KCl, and 10 mM $MgCl_2$ using ITC at 303 K as described in the Materials and Methods.

interfere with the formation of other protein−ligand interactions. Normally, in the enzyme−ADP complex, the distance between the amide nitrogen of Ala93 and N1 of the adenine ring is 2.83 Å.

In purine riboside, the amino group of the adenine ring has been removed and the electrostatic potential surface of this analogue (Figure 5) illustrates that the purine ring system is lacking the electropositive hydrogen atoms of the amino group. In the adenine ring, these hydrogen atoms are involved in hydrogen-bonding interactions with residues 90−93 of the enzyme (Figure 1). The enthalpic contribution of purine riboside binding to the enzyme is significantly reduced, and this analogue forms an extremely weak complex with APH(3′)-IIIa.

Addition of a halogen atom to the adenine ring, as in 8-bromoadenosine and 2-chloroadenosine, lead to analogues that have lower K_d values and enzymes complexes that are more entropically favored. The electrostatic potential surfaces of these analogues (Figure 5) predict that a small amount of electron density has been pulled away from specific nitrogen atoms in the heteroaromatic systems toward the electronegative halogen atoms.

DISCUSSION

Previous studies have suggested that nucleotide binding to APH(3′)-IIIa is governed by enthalpic forces (*6*) primarily through electrostatic $\pi-\pi$ stacking and hydrogen-bonding type interactions, in contrast to nucleotide/inhibitor binding to structurally similar ePKs, where ligand binding has been primarily described as "hydrophobic" (*8*, *11*, *25*). Calculations on the nucleotide-binding region of this enzyme, along with a thermodynamic comparison of adenosine binding to APH(3′)-IIIa WT and Met90 mutants, have further highlighted the electrostatic nature of nucleotide binding. Met90 appears to be part of a polar network of hydrogen bonds used to recognize the adenine ring of the bound nucleotide. Although Met90 is not completely conserved in the APH(3′) protein family, it is generally replaced with Thr, another amino acid capable of providing a similar hydrogen-bonding interaction through its side chain.

The ITC results with the Met90 mutants are especially intriguing because the specificity of inhibitor binding to protein kinases has been associated with the size and nature of the "hydrophobic" pocket that encompasses Met90 or equivalent amino acids (*8*, *11*, *25*). Furthermore, mutation of Met90 equivalents significantly alters inhibitor sensitivity and selectivity (*12*, *26*, *27*), leading researchers to term this amino acid the gatekeeper residue. The work described in this paper indicates that ligand binding to ePKs that also has Met or a similarly capable hydrogen-bond donor/acceptor residue at this position may also have an important polar component to their free-energy profile, and inhibitor sensitivities may be in part because of differing hydrophobic−electrostatic potentials of their ATP-binding sites. This suggests that the inhibitor selectivity because of the gatekeeper residue is not solely based on steric clash but may involve hydrogen bonding or other polar contacts in this important binding pocket. Further exploitation of these additional characteristics of the gatekeeper residue in APHs and ePKs will lead to more specific, higher affinity inhibitors.

The calorimetric and computational studies with the adenosine analogues have also revealed important structural and electronic factors necessary for recognition in the adenine-binding site of APH(3′)-IIIa. As noted, these results are not only important for APH(3′)-IIIa but also for other adenine-binding proteins, considering the importance of hydrogen-bonding and $\pi-\pi$ stacking interactions in other protein systems. For example, one recent data mining study suggested that 59 and 65% of the adenylate−protein complexes in the PDB had a similar hydrogen-bonding scheme and a $\pi-\pi$ stacking interaction, respectively (*1*). With this in mind, APH(3′)-IIIa can serve as an excellent experimental model system, and our computational/mutagenesis/calorimetric approach is among the first attempts to better understand how these interactions act in concert to recognize the adenine ring (*6*). The stacking of nucleic acid bases and supporting hydrogen-bonding interactions have been intensely investigated for many years (*4*, *28*−*31*). It is imperative that hydrogen-bonding and $\pi-\pi$ interactions within purine/pyrimidine-binding sites in proteins receive the same level of attention.

As in many binding studies, there was some enthalpy−entropy compensation observed in the thermodynamic values for the various adenosine analogues. However, if electrostatic interactions play a key role in adenine binding to this enzyme (*6*), such compensation would not be unexpected. In our

Table 3: Thermodynamic Parameters for Interactions between APH(3′)-IIIa WT and Adenosine Compounds[a]

compound	K_d (μM)	ΔG (kcal/mol)	ΔH (kcal/mol)	$-T\Delta S$ (kcal/mol)
adenosine	11.0 ± 0.1	−6.88 ± 0.01	−17.5 ± 0.07	+10.6 ± 0.08
8-bromoadenosine	2.43 ± 0.11	−7.78 ± 0.02	−11.8 ± 0.02	+4.03 ± 0.05
2-chloroadenosine	4.72 ± 0.09	−7.38 ± 0.01	−11.8 ± 0.30	+4.42 ± 0.35
7-deazaadenosine	38.2 ± 1.9	−6.13 ± 0.03	−13.6 ± 0.26	+7.45 ± 0.13
3-deazaadenosine	56.3 ± 0.2	−5.89 ± 0.01	−15.6 ± 0.02	+9.69 ± 0.03
1-deazaadenosine[b]	>2000			
purine riboside[c]	727	−4.35 ± 0.94	−8.08 ± 1.75	+3.73 ± 0.81

[a] The values determined in 50 mM HEPES-NaOH at pH 7.5, 40 mM KCl, and 10 mM $MgCl_2$ using ITC at 303 K as described in the Materials and Methods. [b] No binding of 1-deazaadenosine to the enzyme was detected in ITC experiments; no inhibition of APH(3′)-IIIa activity was observed in enzyme kinetic studies up to 2 mM. [c] The values for purine riboside are only an approximation because the parameters were determined by manually adjusting the K_d to find the best fit to the ITC curve.

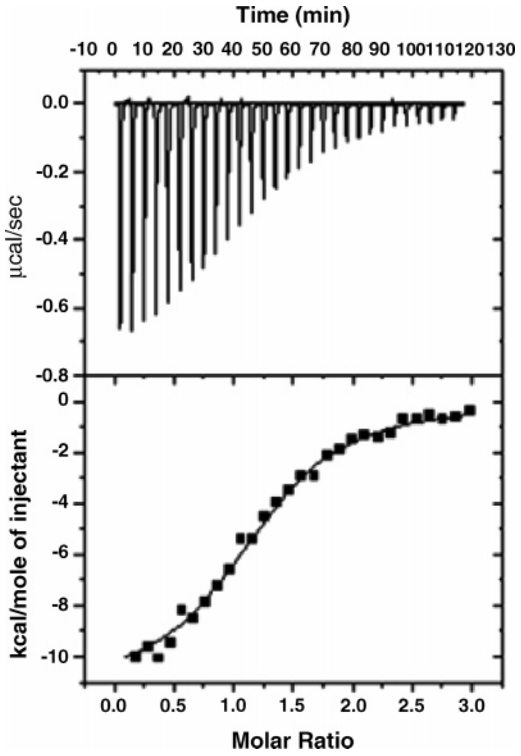

FIGURE 4: Isothermal calorimetric titration for the interaction between 8-bromoadenosine and APH(3′)-IIIa. (top) Raw data for 28 10-μL injections of 8-bromoadenosine (0.2 mM stock) into the isothermal cell containing 15 μM APH(3′)-IIIa WT at 4 min intervals and 30 EC. Both the protein and ligand were in 50 mM HEPES-NaOH at pH 7.5, 40 mM KCl, and 10 mM $MgCl_2$. (bottom) Experimental points were obtained by the integration of the above peaks and plotted against the molar ratio of 8-bromoadenosine/protein in the reaction cell.

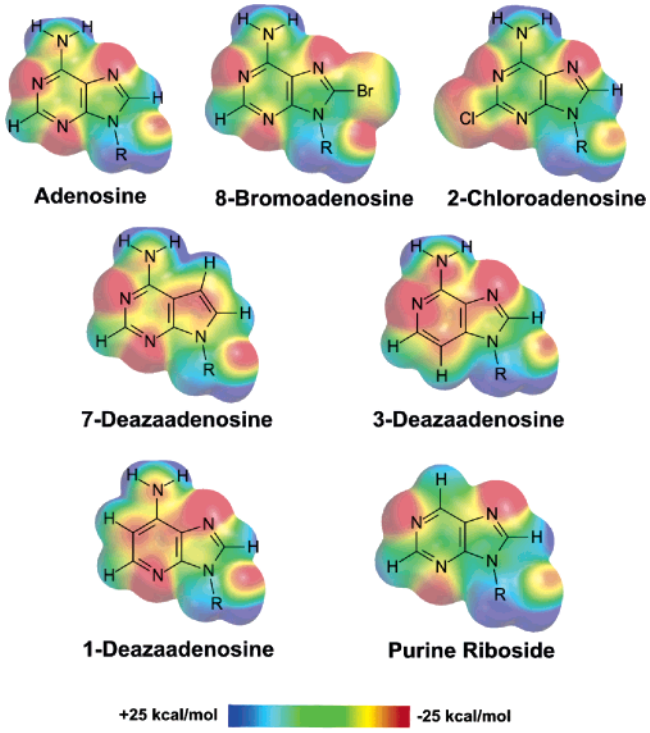

FIGURE 5: Electrostatic potential surfaces of model systems used to represent the indicated nucleosides. In all of the structures, the R group represents the ribose ring. For computational purposes, the R group was a $-CH_2OH$ and the positions of the anomeric carbon and oxygen were derived from the coordinates of bound ADP in the APH(3′)-IIIa−ADP complex (5). The potential energy extremes in the electrostatic map are from −25 to +25 kcal/mol. The color red indicates areas of greater electron density, while blue indicates areas of less electron density. From negative to positive potentials, the colors progress red−orange−yellow−green−cyan−blue.

calorimetric experiments, we systematically removed polar regions from the enzyme (Met90) or the adenine ring (adenosine analogues) and monitored binding. After removal of these polar regions via enzyme or molecular mutagenesis, enzyme−nucleoside complex formation is more hydrophobic in nature and entropic effects are expected to play a more prominent role (*14*).

For this reason, we were not able to assign energetic or thermodynamic values to specific contacts in the adenine-binding region of APH(3′)-IIIa. However, there were significant and reproducible changes in enzyme−nucleoside affinity upon mutagenesis of Met90 or the adenine ring of adenosine. In addition, the enthalpy contribution to binding becomes less favorable as the opportunity for electrostatic complementarity is diminished, which suggests that polar interactions in the adenine-binding region are important. This type of information can help guide the synthesis of ATP-mimics that encompass the important defined electrostatic/hydrophobic characteristics to specifically and efficiently inhibit APH(3′) enzymes. For instance, the results with the 1-deazaadenosine and purine riboside demonstrate the need for aromatic systems to have both the proper balance of electrostatics and size to be recognized in the adenine-binding region of APH(3′)-IIIa. Moreover, molecular modeling of the halogenated ring systems in the adenine-binding pocket (not shown) suggests that it is unlikely they can adopt the same arrangements as the adenine ring of adenosine because of steric clashes with atoms of the enzyme, and thus , it appears that alternative binding modes can still lead to tight-binding complexes with APH(3′)-IIIa.

CONCLUSIONS

Our investigation into the nucleotide-binding site of APH(3′)-IIIa has highlighted the importance of the contact between the adenine ring and Met90. Computational and calorimetric experiments involving site-directed and molecular mutagenesis all point to the polar nature of this interaction. This contact is among other hydrogen bonds and a $\pi-\pi$ interaction employed by APH(3′)-IIIa to recognize the adenine ring. Typically, Met residues in the adenine-binding regions of protein kinases are considered gatekeeper residues that reside in a hydrophobic pocket. Therefore, Met residues in the adenine-binding regions of kinases may play a structural role in a hydrophobic pocket or serve as hydrogen-bond acceptors in more polar binding pockets such as the adenine-binding region of APH(3′)-IIIa.

In real biological systems, the disruption of a single contact can influence the nature of the remaining contacts, and thus, systems must be treated in whole rather than by summing their constituent parts. Therefore, this study serves as a caution when trying to compare small-molecule model systems to their more complex protein−ligand counterparts. In the latter case, there are a variety of interconnected, noncovalent interactions, and disturbance of one of these contacts can significantly impact the relative contribution of the others in determining protein−ligand binding. Even nonconserved amino acid residues, such as Met90 in APH(3′)-IIIa, have important roles to play in determining the relative contributions of enthalpy- and entropy-type forces. Although "energy" cannot be simply divided up into individual contacts, we have shown that the binding of adenine to this aminoglycoside kinase is through directed, enthalpy-based forces, not simply structural complementarity and associated entropy-type forces observed in other kinases.

Overall, this work has highlighted an important distinction between aminoglycoside and protein kinases and provides a foundation in which to further develop compounds that specifically block the binding of ATP to APH-type enzymes, the first step in the catalytic cycle of this family of enzymes involved in antibiotic resistance. In particular, 2-chloroadenosine and 8-bromoadenosine are the highest affinity, ATP-site directed inhibitors of aminoglycoside kinases discovered to date ($K_d < 5\ \mu M$), and when tethered to an appropriate aminoglycoside mimic, they have the potential to provide sufficient selectivity and potency to overcome aminoglycoside resistance *in vivo*.

ACKNOWLEDGMENT

The authors thank Dr. Raquel Epand for her continuing assistance with the ITC experiments. Support of the National Institutes of Health and the National Center for Research Resources Grant (P20-RR16481), which established the Kentucky Biomedical Research Infrastructure Network, is also acknowledged.

REFERENCES

1. Mao, L., Wang, Y., Liu, Y., and Hu, X. (2004) Molecular determinants for ATP-binding in proteins: A data mining and quantum chemical analysis, *J. Mol. Biol. 336*, 787−807.
2. Wright, G. D., and Thompson, P. R. (1999) Aminoglycoside phosphotransferases: Proteins, structure, and mechanism, *Front. Biosci. 4*, D9−D21.
3. Kryger, G., Silman, I., and Sussman, J. L. (1999) Structure of acetylcholinesterase complexed with E2020 (Aricept): Implications for the design of new anti-Alzheimer drugs, *Struct. Fold Des. 7*, 297−307.
4. Meyer, E. A., Castellano, R. K., and Diederich, F. (2003) Interactions with aromatic rings in chemical and biological recognition, *Angew. Chem. Int. Ed. 42*, 1210−1250.
5. Burk, D. L., Hon, W. C., Leung, A. K., and Berghuis, A. M. (2001) Structural analyses of nucleotide binding to an aminoglycoside phosphotransferase, *Biochemistry 40*, 8756−8764.
6. Boehr, D. D., Farley, A. R., Wright, G. D., and Cox, J. R. (2002) Analysis of the $\pi-\pi$ stacking interactions between the aminoglycoside antibiotic kinase APH(3′)-IIIa and its nucleotide ligands, *Chem. Biol. 9*, 1209−1217.
7. Hon, W. C., McKay, G. A., Thompson, P. R., Sweet, R. M., Yang, D. S., Wright, G. D., and Berghuis, A. M. (1997) Structure of an enzyme required for aminoglycoside antibiotic resistance reveals homology to eukaryotic protein kinases, *Cell 89*, 887−895.
8. Williams, D. H., and Mitchell, T. (2002) Latest developments in crystallography and structure-based design of protein kinase inhibitors as drug candidates, *Curr. Opin. Pharmacol. 2*, 567−573.
9. Traxler, P., Bold, G., Buchdunger, E., Caravatti, G., Furet, P., Manley, P., O'Reilly, T., Wood, J., and Zimmermann, J. (2001) Tyrosine kinase inhibitors: From rational design to clinical trials, *Med. Res. Rev. 21*, 499−512.
10. Habeck, M. (2002) FDA licences imatinib mesylate for CML, *Lancet Oncol. 3*, 6.
11. Toledo, L. M., Lydon, N. B., and Elbaum, D. (1999) The structure-based design of ATP-site directed protein kinase inhibitors, *Curr. Med. Chem. 6*, 775−805.
12. Cohen, M. S., Zhang, C., Shokat, K. M., and Taunton, J. (2005) Structural bioinformatics-based design of selective, irreversible kinase inhibitors, *Science 308*, 1318−1321.
13. Zhang, C., Kenski, D. M., Paulson, J. L., Bonshtien, A., Sessa, G., Cross, J. V., Templeton, D. J., and Shokat, K. M. (2005) A second-site suppressor strategy for chemical genetic analysis of diverse protein kinases, *Nat. Methods 2*, 435−441.
14. Chakrabarti, P., and Uttamkumar, S. (1995) CH/π interaction in the packing of the adenine ring in protein structures, *J. Mol. Biol. 251*, 9−14.
15. McKay, G. A., Thompson, P. R., and Wright, G. D. (1994) Broad spectrum aminoglycoside phosphotransferase type III from *Enterococcus*: Overexpression, purification, and substrate specificity, *Biochemistry 33*, 6936−6944.
16. Wiseman, T., Williston, S., Brandts, J. F., and Lin, L. N. (1989) Rapid measurement of binding constants and heats of binding using a new titration calorimeter, *Anal. Biochem. 179*, 131−137.
17. Antonini, I., Cristalli, G., Franchetti, P., Grifantini, M., Martelli, S., and Petrelli, F. (1984) Deaza analogues of adenosine as inhibitors of platelet aggregation, *J. Pharm. Sci. 73*, 3666−3669.
18. Cristalli, G., Franchetti, P., Grifantini, M., Vittori, S., Bordoni, T., and Geroni, C. (1987) Improved synthesis and antitumor activity of 1-deazaadenosine, *J. Med. Chem. 30*, 1686−1688.
19. Jeffrey, G. A. (1997) *An Introduction to Hydrogen Bonding*, Oxford, New York.
20. Gregoret, L. M., Rader, S. D., Fletterick, R. J., and Cohen, F. E. (1991) Hydrogen bonds involving sulfur atoms in proteins, *Proteins 9*, 99−107.
21. McKay, G. A., and Wright, G. D. (1995) Kinetic mechanism of aminoglycoside phosphotransferase type IIIa. Evidence for a Theorell−Chance mechanism, *J. Biol. Chem. 270*, 24686−24692.
22. McKay, G. A., and Wright, G. D. (1996) Catalytic mechanism of enterococcal kanamycin kinase (APH(3′)-IIIa): Viscosity, thio, and solvent isotope effects support a Theorell−Chance mechanism, *Biochemistry 35*, 8680−8685.
23. Özen, C., and Serpersu, E. H. (2004) Thermodynamics of aminoglycoside binding to aminoglycoside−3′-phosphotransferase IIIa studied by isothermal titration calorimetry, *Biochemistry 43*, 14667−14675.
24. Leavitt, S., and Freire, E. (2001) Direct measurement of protein binding energetics by isothermal titration calorimetry, *Curr. Opin. Struct. Biol. 11*, 560−566.
25. Noble, M. E., Endicott, J. A., and Johnson, L. N. (2004) Protein kinase inhibitors: Insights into drug design from structure, *Science 303*, 1800−1805.
26. Bishop, A. C., Buzko, O., and Shokat, K. M. (2001) Magic bullets for protein kinases, *Trends Cell Biol. 11*, 167−172.

27. Niswender, C. M., Ishihara, R. W., Judge, L. M., Zhang, C., Shokat, K. M., and McKnight, G. S. (2002) Protein engineering of protein kinase A catalytic subunits results in the acquisition of novel inhibitor sensitivity, *J. Biol. Chem. 277*, 28916−28922.
28. Kool, E. T., Morales, J. C., and Guckian, K. M. (2000) Mimicking the structure and function of DNA: Insights into DNA stability and replication, *Angew. Chem. Int. Ed. 39*, 990−1009.
29. Guckian, K. M., Schweitzer, B. A., Ren, R. X.-F., Sheils, C. J., Tahmassebi, D. C., and Kool, E. T. (2000) Factors contributing to aromatic stacking in water: Evaluation in the context of DNA, *J. Am. Chem. Soc. 122*, 2213−2222.
30. Luo, R., Gilson, H. S. R., Potter, M. J., and Gilson, M. K. (2001) The physical basis of nucleic acid base stacking in water, *Biophys. J. 80*, 140−148.
31. Friedman, R. A., and Honig, B. (1995) A free energy analysis of nucleic acid base stacking in aqueous solution, *Biophys. J. 69*, 1528−1535.

BI051085P